Electrical resistivity tomography used to characterize bubble distribution in complex aerated reactors: Development of the method and application to a semi-industrial MBR in operation

E. Suard[a], R. Clément[b], Y. Fayolle[a,*], M. Alliet[c], C. Albasi[c], S. Gillot[b]

[a] *Irstea, UR HBAN, centre d'Antony, 1 rue Pierre-Gilles de Gennes, F-92761 Antony, France*
[b] *Irstea, UR REVERSAAL, Centre de Lyon-Villeurbanne, F-69625 Villeurbanne Cedex, France*
[c] *Laboratoire de Génie Chimique, Université de Toulouse, CNRS, INPT, UPS, Toulouse, France*

HIGHLIGHTS

- A numerical procedure is proposed to define ERT methodology for reactors with complex geometry.
- ERT was used to study the gas phase distribution in an aerated plant scale-MBR filled with activated sludge.
- ERT is adapted to bubble dispersion characterization in membrane modules with activated sludge.
- The bubble dispersion over the membrane module surface depends on the air flow and MLSS concentration.

GRAPHICAL ABSTRACT

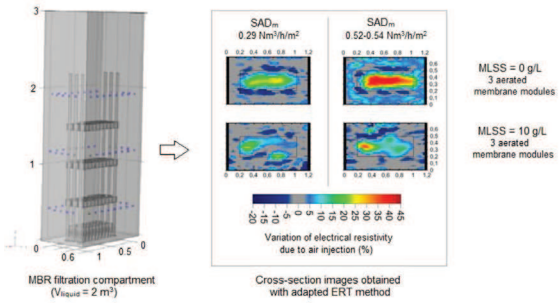

ABSTRACT

Membrane bioreactors (MBRs) are widely used in wastewater treatment processes. However, membrane fouling mitigation remains challenging. Several strategies have been developed industrially to enhance MBR productivity, including coarse bubble aeration. The way such aeration participates in hydrodynamic patterns is an important research topic given its major contribution to the energy costs of such facilities. The methods currently used for hydrodynamic characterization suffer from several drawbacks, mainly due to the system's complexity. Consequently, there is a need for a nonintrusive method that could be employed in reactors with complex internal geometry and in the presence of activated sludge.

This article presents the evaluation and adaptation of the electrical resistivity tomography (ERT) to gain insights into hydrodynamic conditions and to determine how bubbles are distributed within membrane bioreactors in different aeration conditions. An approach used by geophysicists was adapted to a semi-industrial MBR: a numerical procedure was used to validate ERT's ability to recover precise information in a complex geometry such as MBR membrane tank.

Experiments were conducted in a semi-industrial membrane bioreactor with clear water and activated sludge. The resulting images were analyzed in terms of bubble dispersion over a section of the pilot. Heterogeneities were detected in all configurations studied in numerical simulations, although the results also emphasize the diffuse character of gas distribution obtained with the ERT method. Experimental results highlight how gas distribution is mainly localized inside membrane modules and its homogeneity over the module depends on activated sludge rheological properties and air flow rate. MBR operation could be optimized by considering the

operating conditions which provide efficient gas distribution over the membrane module obtained at a scale representative of industrial reactors.

1. Introduction

Membrane bioreactors (MBRs) are biological wastewater treatment processes, composed of an activated sludge reactor coupled with membrane filtration. Their use has continued to expand for the last two decades given their advantages such as high effluent quality and compactness [1]. However, fouling control of membranes remains a critical issue at the industrial scale [2]. Among the methods employed to prevent fouling, coarse bubble aeration limits deposition of particles on the membrane's surface and reduces fouling. In this way, a sustainable filtration flux can be maintained, but this air injection generates significant operating costs [1]. Consequently, recent research has focused on membrane aeration optimization and more specifically on characterizing the hydrodynamics in such reactors. The main objective has been to gain insight into mechanistic impacts of the aeration strategy on fouling limitation such as turbulence and back transport, and also fiber movement and local shear stress [3]. Such studies are required to identify processes but also to develop experimental databases needed to build models. Particle image velocimetry (PIV) and high-speed cameras have been used to describe fiber movement and bubble distribution at several gas flow rates at the laboratory scale [4,5] and the semi-industrial scale [6,7,8]. The electrochemical method, using an electrolyte solution and shear probes embedded in test fibers [7,9,10] and PIV [5], have been used to monitor shear stress at the membrane's surface. However, the application of such methods requires specific fluid characteristics such as transparency or electrochemical properties and cannot be operated in presence of activated sludge. On the other hand, the impact of rheology on bubble size, shape and preferential flow path have been reported [4,11] and should not be neglected. Braak et al. [12] compared hydrodynamics between air/water and air/mixed liquor flows. They found velocities lower in the activated sludge than in the water for the air flow rates tested and shear stresses were one order of magnitude higher in activated sludge than in water. Review papers have also mentioned the importance of activated sludge rheology on hydrodynamics [13,14] and the scale-up problems transferring lab-scale experimental observations to large-scale MBRs [14,15]. Alternative investigation methods must be developed to characterize gas–liquid hydrodynamics in MBRs under representative operating conditions in terms of reactor size, fiber density and fluid properties.

Alternatively, electrical resistivity tomography (ERT) could overcome these limitations. Through current injections and voltage measurements, ERT allows the reconstruction of conductivity distributions as well as electrical impedance resistivity (EIT). The main difference between those two techniques being how the current is injected (alternating current for EIT and direct current for ERT). This technique has been widely applied in the field of conventional chemical engineering and is well adapted to study phase distribution and mixing performance considering two or three phases with different conductivities [16]. Geometries studied range from pipe with a diameter of 35 mm to mixing vessels with a diameter of 1.5 m. Generally, the authors emphasized the need to widen the scope of media studied, which was mostly water for the liquid phase even though some papers dealt with xantham gum [17,18]. Sharifi and Young [16] advised to investigate fluids common in the food industry but also wastewater. Consequently, the electrical tomography measurement seems to be a convenient candidate to gain insight into gas distribution inside a MBR for different aeration strategies.

More recent studies have used EIT to analyze mixing performance and gas hold up inside a bubble column containing activated sludge [19,20]. Most of these studies used electrode rings composed of 16 electrodes and implemented the adjacent electrode pair strategy. The EIT measurements were taken using a frequency current of 9.6 kHz in most cases. However, the authors identified some gaps in the literature: ERT and EIT could be used as monitoring tools at industrial scale but some developments to improve accuracy, measurement frequency and robustness were still needed [16]. In most cases, the ERT and EIT are applied to simple reactor configuration with similar experimental procedure in terms of amount of implemented electrodes and applied electrode arrays. However, in case of complex reactor geometries, such as MBR with presence of membranes, the experimental methodology of ERT and EIT must be thoroughly adapted and validated considering specific geometries.

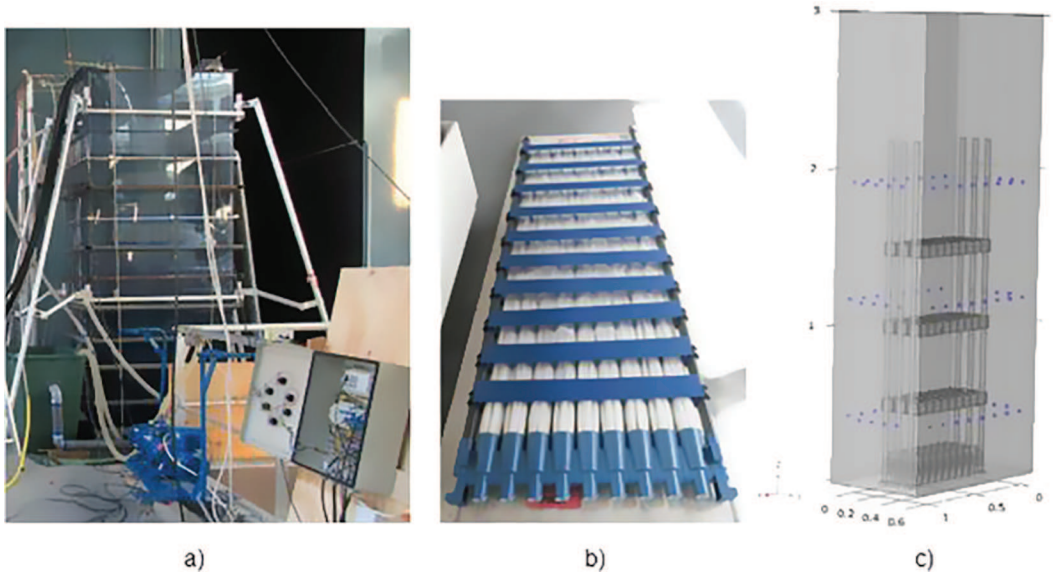

Fig. 1. a) Semi-industrial MBR, b) KMS Puron membrane module, c) pilot geometry and electrode locations (blue). (For interpretation of the references to colour in this figure legend, the reader is referred to the web version of this article.)

In near-surface geophysics, a substantial literature uses the ERT method to characterize the ground and hydrodynamic transfers that may occur in the soil at a large scale [21,22,23]. However, for geoscience applications, measurements are usually composed of a large number of quadripoles and the measurement may last several hours, in accordance with systems dynamics. It is therefore necessary to adapt the measurement sequence to obtain a short acquisition time, more appropriate to the study of aeration strategy impact on bubble distribution. Nevertheless, an effort should be made to conserve an efficient image reconstruction. For such application, the design of electrodes configuration can be supported using numerical study to guarantee a precise description of the evolution of studied systems [24].

This paper is original in that it adapts direct current electrical resistivity tomography (ERT) to study gas dispersion in a semi-industrial MBR (filtration compartment: 2 m^3 pilot) filled with activated sludge. To this aim, a classical geophysical methodology based on numerical study [24] was followed to adapt the ERT method to a complex and semi-industrial scale aerated reactor. The adaptation of the method as well as its validation through numerical study of theoretical cases is presented in a first part. Then the validated ERT method was implemented on the filtration compartment to observe bubble dispersion for activated sludge at several mixed liquor suspended solid concentrations and its potential to detect a liquid phase influence on bubble dispersion is experimentally evaluated in the second part of this paper.

2. Materials and methods

2.1. Semi-industrial filtration compartment (pilot)

2.1.1. Pilot characteristics

A semi-industrial PVC reactor (V_{liquid} = 2.0 m^3, L × l × h_{liquid} (m) = 1.23 × 0.70 × 2.40, Fig. 1a) was equipped with three hollow fiber membrane modules (KMS Puron, PSH 34, Fig. 1b, filtration surface = 3 × 34 m^2 = 102 m^2). Each membrane module consists of nine fiber bundles, as illustrated in Fig. 1b.

The reactor was continuously filled with activated sludge (mixed liquor suspended solid (MLSS) concentration = 6 and 10 g/L) or clear water, and filtration occurred at a liquid flow rate of 1.3 m^3/h. Fresh activated sludge was sampled from one of the reactors of the Seine Aval water resource recovery facility (WRRF) treating rejection water from the sludge treatment. A complementary experiment was conducted at a MLSS concentration of 3 g/L (obtained by diluting activated sludge with tap water). For this specific concentration, measurements were taken without filtration or activated sludge filling in order to maintain the MLSS concentration in the bioreactor.

2.1.2. Aeration conditions

The injectors of coarse bubbles are located at the bottom center of each fiber bundle. The operating conditions of the semi-industrial MBR are described in Table 1. For experiments A to D, air flow rates were chosen in the range of advised industrial SAD_m (specific aeration demand, the ratio between the air flow rate and membrane area in filtration) between 0.27 and 0.60 $Nm^3/h/m^2_{membrane\ area}$. For experiment with only one aerated membrane module and three modules in filtration (Experiment E), the SAD_m was in the 0.14–0.18 $Nm^3/h/m^2_{membrane\ area}$ range in order to keep the same air flow rate per module. For each aeration strategy, a preliminary reference measurement without aeration was performed.

Temperature (T), conductivity (σ) and MLSS concentration ([MLSS]) were regularly measured during the experiment. The main values of these parameters are presented in Table 1. Activated sludge samples were collected during the overall period of the semi-industrial pilot monitoring for measurements of particle size distribution and rheology, using laser granulometer (Malvern MASTERSIZER 3000) and tubular rheometer [25], respectively.

2.2. ERT method and applied general methodology

The apparent electrical resistivity (Eq.1) is determined from a measurement of potential difference between two electrodes M and N (called potential electrodes), resulting from a current injection between two electrodes A and B (called injection electrodes). The combination of these four electrodes (two injection and two potential electrodes) is called a quadripole. The resulting electrical resistivity is called apparent and it differs from the true electrical resistivity due to studied media heterogeneity. Also, an inversion step is needed for image reconstruction of interpreted electrical resistivity (ER) distribution (see II.2.2).

$$\rho_{app} = \frac{kX\Delta V_{MN}}{I_{AB}} \quad (1)$$

with ρ_{app} the apparent electrical resistivity (Ω.m), ΔV_{MN} the electrical potential difference measured between electrodes M and N (V), I_{AB} the intensity of the injected current between electrodes A and B (A), and k the geometric factor (m).

The geometric factor k depends on the position and the distance between the four electrodes composing the quadripole and the geometry of the reactor. This geometric factor k, specific to each quadripole, could be determined by two methods [26]: (i) from the experimental apparent ER data set on homogeneous medium (in our study, the measurements were done for the semi-industrial pilot filled with tap water and without membrane) or (ii) from numerical modeling (as indicated in Section 2.3.2) of a case considering an homogeneous ER distribution on the given surface.

The proposed general methodology, presented in Fig. 2, stems from a classical geophysical approach described in Radulescu et al. [24], which provides robust ERT measurements [27] and aims at characterizing the bubble dispersion in a filtration compartment.

First, a numerical study is conducted to assess the ability of the ERT method to recover precise values of electrical resistivity (ER) in theoretical ER distributions. To this purpose, a simplified geometry is created to model the bioreactor outlines. Different scenarios are conceptualized and consist in electrical resistivity values which are attributed to each element in order to represent the gas–liquid mixture within the membranes or surrounding them. Several theoretical ER distributions are then obtained.

To limit acquisition time, the number of electrodes should be restricted and the adapted sequences of quadripoles should be compatible

Table 1
Operating conditions in the semi-industrial MBR.

Exp	[MLSS] (g/L)	Number of aerated membrane modules	SAD_m ($Nm^3/h/m^2$)	T (°C)	σ ($mS.cm^{-1}$)
A	0	3	0.29/0.38/0.52	24	0.7
B	3	3	0.29/0.41/0.46	27	2.2
C	6	3	0.29/0.41/0.47	35	4.5
D	10	3	0.29/0.42/0.54	33	4.4
E	6	1	0.14/0.18	33	4.4

With: T = Temperature (°C), σ = conductivity ($mS.cm^{-1}$), SAD_m = specific aeration demand, the ratio between the air flow rate and membrane area in filtration ($Nm^3/h/m^2$).

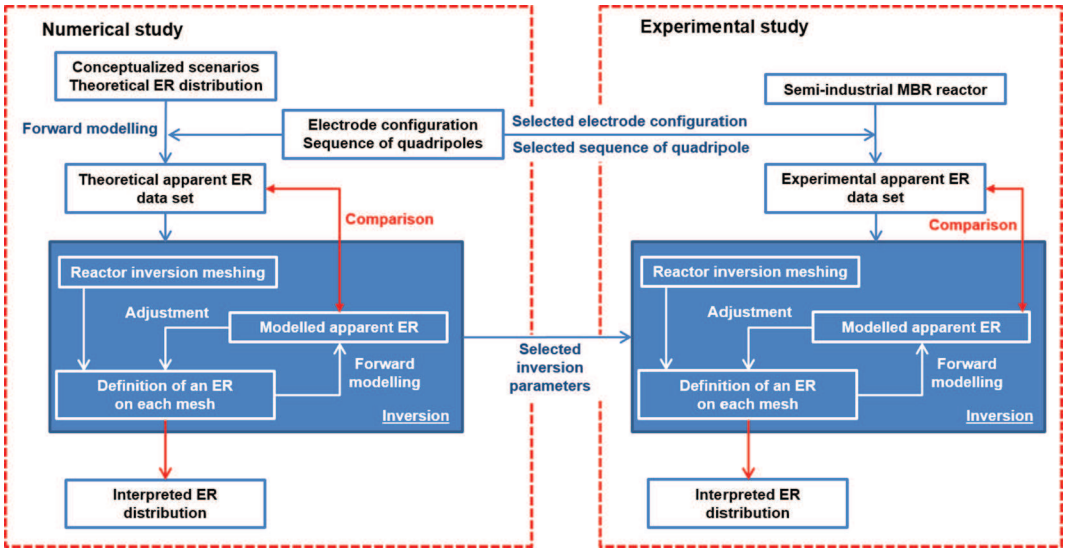

Fig. 2. General methodology of the numerical study and the experimental one.

with multichannel acquisition. Considering these technical constraints, two different electrode arrays are selected to build two sequences of quadripoles (detailed in Section 2.3.4). These sequences are then tested to adapt the ERT method to the complex geometry and dynamics of the semi-industrial MBR. Through forward modeling with these sequences, theoretical apparent ER data sets are generated. These apparent ER data sets are then inverted to obtain interpreted ER distribution which corresponds to the resistivity distribution all over the surface of the reactor. The resulting interpreted ER distributions are finally compared with the theoretical ER distributions to evaluate the relevance of the chosen inversion parameters and electrode arrays used for building the sequences of quadripoles.

Following these numerical developments, experiments are conducted on a semi-industrial filtration compartment filled with water or activated sludge to obtain gas distribution for several operating conditions.

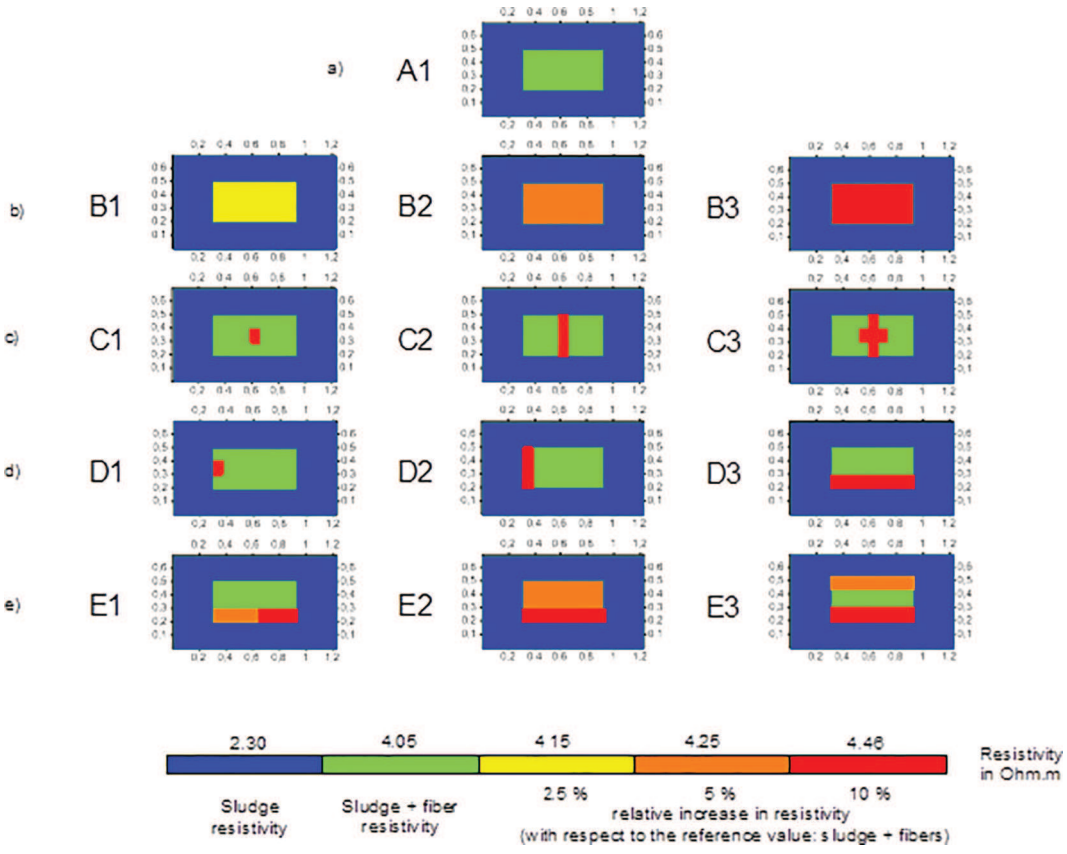

Fig. 3. Horizontal cross sections of theoretical ER distributions.

2.3. ERT numerical study

2.3.1. Definition of theoretical ER distributions: conceptualized scenarios

The numerical study is performed to estimate the ability of the ERT method to recover theoretical ER distributions in a large and complex system.

First, a simplified geometry was defined using the COMSOL software to mimic the characteristics of the membrane bioreactor. A first block (Block 1 – L × l × h (m) = 1.2 × 0.7 × 2.4) was drawn to represent the experimental reactor volume filled with activated sludge. A second block at the center of the reactor volume was used to represent the zone occupied by the membrane modules (Block 2 – L × l × h (m) = 0.83 × 0.3 × 2.4) and was divided into 27 (9 × 3) volumes to represent the location of each fiber bundle. This geometry allows the generation of several theoretical ER distributions including zones with different electrical resistivity values while keeping the same mesh for each simulation. The mesh size of the geometry was reduced iteratively until variations between computed values were lower than 0.05%. To limit calculation time, the less refined meshing validating this condition was selected for forward modeling.

Then an ER value was attributed to each geometrical block to simulate several distributions of electrical resistivity inside the membrane module zone and to evaluate the sensitivity of ERT inversion for each theoretical ER distribution. For each scenario, an ER value (2.3 Ω.m) was attributed to Block 1 in each case to represent the liquid phase. Since ER is the inverse of conductivity, this value was determined from conductivity measurement previously performed on the activated sludge using a conductivity probe (WTW, TetraCon® 325).

The electrical resistivity of the individual elements in Block 2 was set at 4.05, 4.15, 4.25 or 4.46 Ω.m to simulate zones of the membrane module with and without aeration for different gas hold-up values. In first approximation, according to Maxwell equations, positive ER variations of 2.5, 5 and 10% limited on Block 2 correspond to scenarios with local gas hold up of 1.6, 3.2 and 6.3%, respectively. These values are in the range of global gas hold up estimated for the aeration strategy considered, in the semi-industrial pilot filled with activated sludge.

Cross sections of theoretical ER distributions are presented in Fig. 3. The theoretical ER distribution used as a reference (scenario for initial state without aeration) is shown in Fig. 3a and is supposed to represent the zone of the membrane modules without aeration, surrounded by sludge. An ER value is attributed to the whole Block 2 for each theoretical ER distribution presented in Fig. 3b, to stand for homogeneous ER distribution within the membrane module zone. Fig. 3c–e presents ER distributions with heterogeneous ER distributions inside the membrane module zone corresponding to a heterogeneous dispersion of bubbles in the fiber bundles. Small centered and off-center heterogeneities of different sizes are presented in Fig. 3c and 3d, respectively, to evaluate the size detection limit and its sensitivity to distance from the electrodes. Fig. 3e presents theoretical ER distributions created to evaluate the ability of the method to detect different ER values for heterogeneous ER distributions inside the membrane module zone (Block 2).

2.3.2. Forward modeling

The forward modeling is based on the numerical modeling of the potential difference induced by the injected direct current for every selected quadripole.

The governing equation for ERT forward modeling can be derived from Maxwell's equations. Technically ERT is based on a very-low-frequency alternating current (2–5 Hz) to limit polarization effects. In this case, the inductive and capacitive effects in Maxwell's equation could be ignored. Under static conditions, the electric field can be represented by the negative gradient of the electric potential V (Eq.2).

$$E = -\nabla V \tag{2}$$

with E the electric field (V/m) and ∇V the gradient of electric potential (V/m).

In conductive media, to simulate stationary electric current density, the stationary equation of continuity and Ohm's law are considered. In a stationary coordinate system, the point form of Ohm's law states that:

$$J = \sigma E + Je \tag{3}$$

with J is the current density (A/m^2) equal to the current I per unit of cross-sectional area S (A), Je is the externally current density (in A/m^2), E is the electric field intensity and σ is the electrical conductivity (A/Vm or S/m).

The static form of the equation of continuity then states

$$\nabla . J = -\nabla . (\sigma \nabla V - Je) = 0 \tag{4}$$

The generalized form of the current sources (Q_j) can be written as follows:

$$-\nabla . (\sigma \nabla V - Je) = Q_j \tag{5}$$

with Qj is the generalized form of the current sources

Considering the semi-industrial pilot geometry, an insulating boundary condition was applied at the contact area between the homogenous media studied and the semi-industrial pilot, expressed by the Neumann condition. This equation specifies that there is no current flowing across the boundary.

$$n . J = 0 \tag{6}$$

The modeling was performed using COMSOL Multiphysics 5.2a combined with Matlab 2015. With COMSOL, the simplified geometry of the semi-industrial reactor is taken into account and the electrical field distributions can be modeled using full 3D modeling. Electrical field distributions are built using the AC/DC module (quasi-stationary electromagnetic field) to evaluate the potential difference induced by the injected DC current and the electrical boundary conditions selected as infinite or insulating surfaces. This step is made automatically to calculate the electrical potential for every quadripole and every electrical resistivity distribution using F3D-lab Matlab-code (Forward 3D Laboratory) developed by Clement et al. [28]. The script is available from the authors on request. To achieve a realistic data set reflecting the properties of a field survey, apparent electrical resistivity was contaminated with 3% random voltage-dependent noise to simulate a low-noise acquisition.

For more information, the elementary theory of direct current (DC) conductive media modeling can be found in Clement & Moreau [29].

2.3.3. Image reconstruction of interpreted ER distribution from apparent ER data set using inversion procedure

The inversion procedure consists of reconstructing the interpreted electrical resistivity (ER) distribution from the apparent ER data sets.

First, the studied cross-section is divided in a finite amount of elements. In this study, the inversion meshing was refined around the electrodes (minimum cell size = 0.22 cm^2) and the maximum cell size of the cross-section was 2.6 cm^2.

To start, the inversion is initialized by applying an ER distribution (usually a median value of the apparent electrical resistivity) to all cells. Then, an optimization method is used to iteratively change the electrical resistivity of each cell to minimize the difference between the measured and calculated (through forward modeling) apparent ER value (Fig. 2).

In this study, the apparent ER data sets were inverted using a "set as reference" time-lapse procedure used in previous ones [30]. For this time-lapse inversion procedure, the apparent ER data sets for scenarios without gas injection were classically inverted from a homogeneous ER distribution as initial ER distribution. Then, the previously obtained interpreted ER distributions were set as the initial ER for the inversion of the apparent ER data sets for scenarios with gas injection. This procedure is common for most time-lapse surveys, as proposed by Loke [30], Day-Lewis et al. [31] and Vesnaver et al. [32].

To perform 2D time-lapse inversions, BERT software [33] was used with the following parameters: a Gauss–Newton scheme with global regularization was used for the minimization with anisotropic smoothness constraints (horizontal preferential direction), an option to recalculate the Jacobian matrix at each iteration step and a regularization parameter (λ) of 5. Among inversion parameters, the value of the regularization parameter has an influence on the interpreted ER distributions. Low values of λ will produce a highly structured model with huge parameter contrasts and high values of λ will provide smooth ER models [34]. The inversion parameters were optimized and set during the numerical study for the chosen meshing, leading to interpreted ER distributions close to the theoretical ER distributions (optimization not presented here). Consequently, the same inversion meshing and parameters were used for the inversion of the experimental data sets.

The relative root mean square error (rRMS, Eq. (7) was used to determine the misfit between the interpreted data set and the observed data set.

$$rRMS = \sqrt{\frac{\sum_{i=1}^{N} \frac{|(x_{data,i} - x_{model,i}|^2}{|x_{data,i}|^2}}{N}} \quad (7)$$

where $x_{data,i}$ is the measured apparent ER, $x_{model,i}$ the calculated (through forward modeling) apparent ER and N the number of quadripoles.

In the following, results of interpreted ER distributions are presented as Δρ distributions. Δρ is the percentage of ER variation with respect to the ER of the interpreted ER distribution of scenario without gas injection, according to Eq. (8).

$$\Delta\rho = \left(\frac{\rho_f}{\rho_i} - 1\right).\ 100(\%) \quad (8)$$

where ρ_f and ρ_i (in Ω.m) are the ER of the interpreted ER distribution with and without gas injection respectively.

2.3.4. Tested electrode arrays

An electrode array consists of injection (AB) and measurement (MN) dipoles. For each array, the resulting surface investigated depends on the spacing between the current injection electrodes and the distance between the two dipoles. For this study, two electrode arrays were selected to build two sequences of quadripoles, i.e. two lists of associated injection (AB) and measurement (MN) dipoles. In Fig. 4, the 24 electrode locations are indicated by e_i (with i = [1–24]). This number of electrodes was selected from the numerical study, considering a sensitivity analysis of the results to this electrode number. Electrode arrays with 16 electrodes are less efficient to recover theoretical ER distributions than arrays with 24 electrodes, in the center zone of the media corresponding to membrane zone in particular (results not detailed here). As a consequence and to have a short acquisition time in accordance with the bubble dynamics, the number of electrodes was restricted to 24 per cross section (and corresponds to 27.9 electrodes/m^2 of the studied section of the reactor).

The first sequence of quadripoles (DD sequence, principle illustrated in Fig. 4a) was based on the dipole–dipole array [35], which corresponds to the classical electrode array employed in geophysics studies. The measurement (MN) and injection (AB) dipoles are separated and the space between them increased gradually. If injection (AB) and measurement (MN) dipoles consist in two adjacent electrodes (e_i and e_{i+1}), the DD sequence is equivalent to the adjacent electrode pair strategy mentioned in papers examining EIT measurements applied to bubble columns [20,36,37]. The sequence of quadripoles must be adapted for the specific constraints related to the reactor design studied (rectangular shape of the bioreactor, electrode disposition). In geophysics, the number of electrodes between measurement and injection dipoles is generally kept lower than 6 to optimize the signal-to-noise ratio due to a large distance between two dipoles [35]. This was experimentally confirmed as distant injection and measurement dipoles led to more extreme apparent electrical resistivity than other quadripoles, generating artifacts after the inversion step. Therefore, measurement dipole shifting was centered on the injection dipole with a number of electrodes between AB and MN lower than 5 (Fig. 4). This adapted sequence of quadripoles is composed with 300 quadripoles. Injection electrodes A and B are e_i and e_{i+2}, respectively, for the 240 first quadripoles where the injection dipole takes all possible locations (24) while M and N are two consecutive electrodes. The last 60 quadripoles concern 6 combinations of consecutive injection electrodes (e_i and e_{i+1}) regularly distributed around geometry to take into account variations closer to the wall as the depth of investigation increases with increasing spacing between electrodes. Not all 24 locations were considered for consecutive injection electrodes to limit the size of the array and therefore the acquisition time (resulting from analysis not detailed here).

The second sequence of quadripoles (GD, sequence, principle illustrated in Fig. 4.b) is based on the gradient array [35]. Twelve combinations of injection dipoles (opposite position of injection electrodes A and B from e_1-e_{13} to e_{12}-e_{24}, respectively) are considered. Measurement dipole MN is located between the two electrodes of the injection dipole (AB) and takes all the available positions between them (20

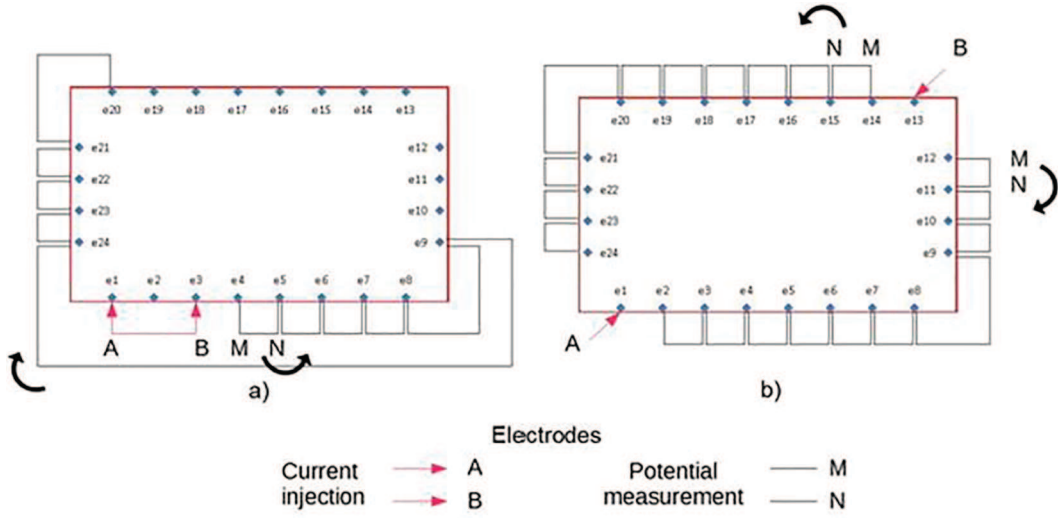

Fig. 4. Adapted sequences based on classical electrode arrays, (a) dipole-dipole (DD) and (b) gradient (GD), with e_i are electrode locations (i = [1–24]).

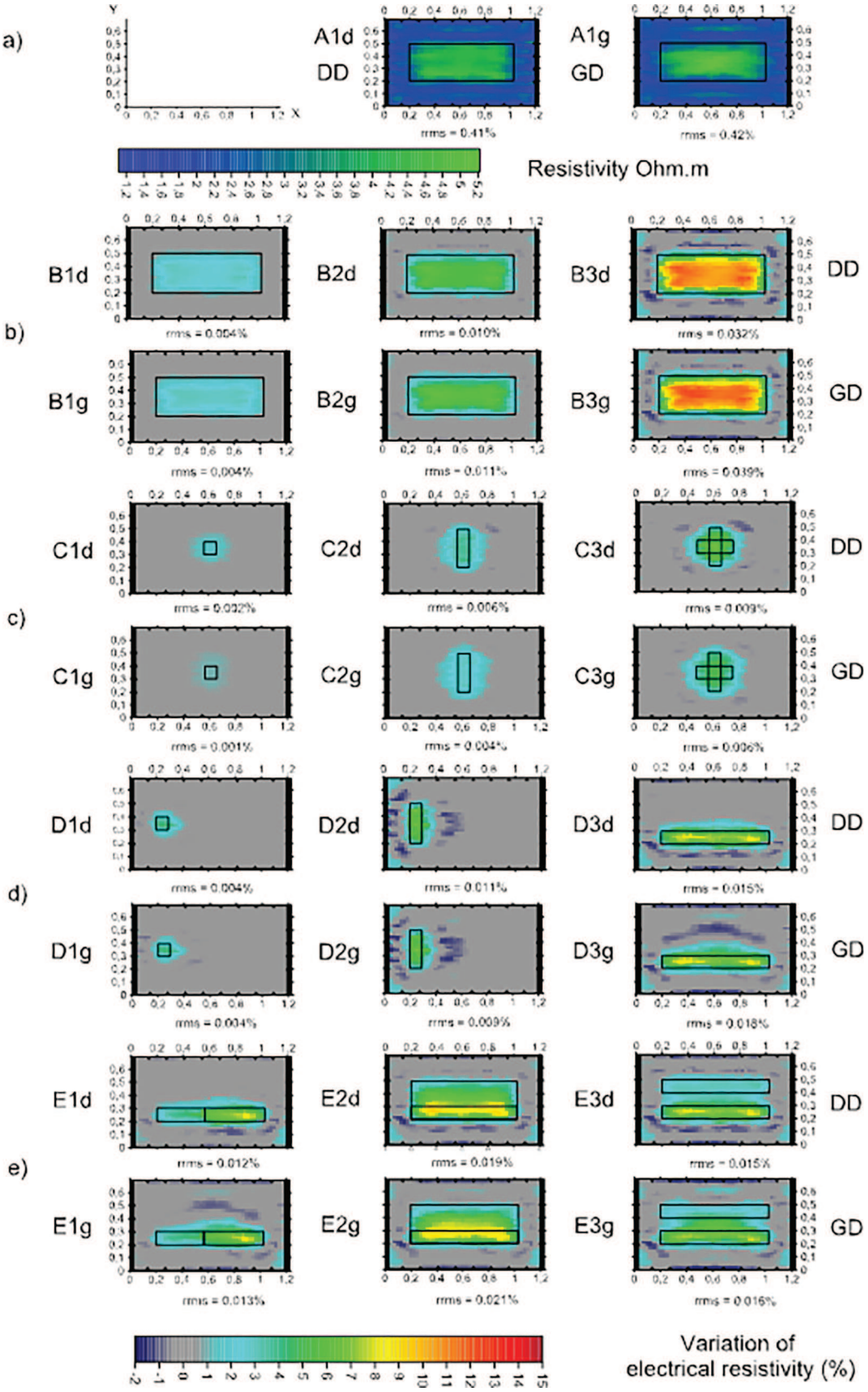

Fig. 5. Initial interpreted ER models and Δρ distributions obtained from numerical simulations – rrms corresponds to relative root mean square error between the modeled and the theoretical apparent ER distribution data sets.

positions). This electrode array, because it considers opposite positions of injection electrodes, is expected to offer better measurement efficiency in the center part of the studied section, ie the zone corresponding to membrane zone and air injection. Each measurement dipole consists of two consecutive electrodes. A total of 240 quadripoles are considered in this case.

2.4. Experimental study: ERT measurements

The electrical imaging survey is carried out using a distribution of electrodes around the reactor. Electrodes were connected to a Syscal Pro (IRIS Instrument, Orléans, France) resistivity meter.

The resistivity meter allows the automatic selection of the quadripoles around the reactor, according to a sequence defined by the user. The multichannel resistivity meter allows to measure the potential resulting from ten potential dipoles during a pulse of current injection between injection electrodes. Consequently, ten quadripoles are measured for one injection current pulse. The injection of current lasts between 150 ms and 8 s. The choice of the injection time value depends on the chargeability of the studied media (i.e., if a medium has the ability to behave like a capacitor, the injection time should be extended).

The stainless steel electrodes were embedded in the reactor walls 0.42 m, 1.17 m and 1.92 m from the bottom (Fig. 2c). According to Clement and Moreau [29], the impact of electrode diameter is considered negligible in the 6–12 mm range, which is the case for the electrodes embedded in the semi-industrial pilot walls (diameter = 8 mm). As determined during the numerical study, the number of electrodes was restricted to 24 per cross section to have a short acquisition time in accordance with the study of bubble dynamics. Several injection times were tested to validate the use of a short time. An injection time of 250 ms was used in the experiments presented in this article, resulting in ERT measurements of total duration around 40 s.

To assess data quality, measurements were carried out in clear water without air injection in the normal and the reciprocal mode [38,39], where current and potential dipoles were switched. According to this methodology, quadripoles associated with apparent electrical resistivity presenting a difference greater than 5% between normal and reciprocal modes were discarded before the inversion step. Among the 300 initial selected quadripoles for the DD sequence, 280 remained for the inversion step. For each measurement, it results in an apparent electrical resistivity data sets composed of 280 individual apparent electrical resistivities.

The inversion of experimental apparent ER data sets was done following the inversion procedure described in Section 2.3.3, applying the same inversion meshing and optimized parameters for the inversion as determined during the numerical study.

3. Results and discussion

3.1. Numerical study

The numerical study was performed in order to evaluate the ability of ERT to recover theoretical ER distributions in conditions equivalent to experimental ones and to validate the efficiency of the sequences of quadripoles presented in Section 2.3.4.

3.1.1. Validation and comparison of sequences of quadripoles

Fig. 5a presents the interpreted ER model obtained from the numerical study based on theoretical ER distribution A1 for the sequences of quadripoles based on DD and GD arrays. Fig. 5b–e presents the results as Δρ distributions obtained from the theoretical ER distributions B1 to E3. Δρ distributions are presented for the two sequences of quadripoles (GD [g] and DD [d]). Theoretical locations of positive Δρ are indicated by rectangular shapes added to each figure.

The interpreted ER distribution A1d shows a more uniform profile than A1g in the zone corresponding to the membrane location. The obtained results for ER and Δρ distributions A1 to E3 replicate each theoretical variation of ER in terms of value and position within the studied surface. However, two remarks should be made. First, the imposed values of resistivity are retrieved when the zone with modified resistivity is large enough (cases B and E2) and calculated values are much smaller than fixed one for small zones (case C1 for example). Secondly, positive Δρ are observed around the delimited theoretical zones, which indicate that the method employed induces a slight diffusion of the information, especially for zones located far from the electrodes.

Fig. 6 presents the vertical Δρ distributions at the center of the cross section for Δρ distributions B3 and D3, as example. A smoothness coefficient is determined, as illustrated in Fig. 6, to estimate the Δρ spreading due to the inversion procedure of the ERT method for each Δρ distribution. Separations between individual elements in block 2 are emphasized by dashed lines in Fig. 6. The smoothness coefficient is defined as the ratio between the lengths of the heterogeneity (defined by $\Delta\rho > 0$) for theoretical and interpreted Δρ distributions, determined from the theoretical center of the heterogeneity along both axes. Therefore, for a smoothness coefficient of 1, the limit of the heterogeneity is efficiently recovered in the numerical interpreted ER

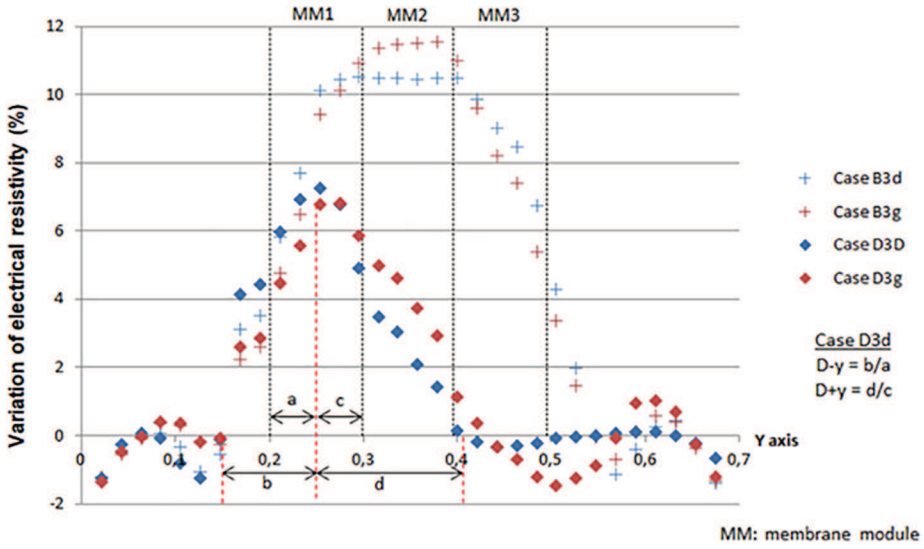

Fig. 6. Vertical Δρ distribution at the center of the cross section for Δρ distributions B3 and D3; illustration of the smoothness coefficient for case D3d.

distribution. As a contrary, a value far from 1 indicates a poor recovery of the limit of the heterogeneity. Four values are available – D_{-x}, D_{+x} and D_{-y}, D_{+y} for the X- and Y-axes, respectively – to study the symmetrical or asymmetrical character of the spread depending on the heterogeneity location. These coefficients for most Δρ distributions illustrated in Fig. 5 are presented in Table 2.

As seen in Fig. 5 and Table 2, the diffusion is less significant when the heterogeneity is close to the electrodes. For example, the smoothness coefficient for Δρ distribution D1d ranges from 2.7 on the electrode side (D_{-x}) to 5 towards the center of the cross section (D_{+x}) for the DD sequence, which is similar to the GD sequence (Δρ distribution D1g). Moreover, in case of small-centered heterogeneity (C1d and C1g), smoothness coefficients are higher in the X-direction than in the Y-direction, which supports the hypothesis of a relationship between diffusion and the distance to the electrodes since X is longer than Y for the cross section studied here.

Fig. 6 also presents Δρ values along the Y-axis for Δρ distributions B3d and B3g. These two distributions are the results for a theoretical ER distribution with a 10% ER difference for Block 2 with respect to the initial theoretical ER distribution (see Section 2.3.1). Maximum Δρ are closer to the modeled 10% difference in these two Δρ distributions compared with Δρ distributions D3d and D3g. As illustrated in Fig. 5 by the color used to represent the ER variations, the higher the smoothness coefficient, the lower the Δρ obtained. This way, the mean Δρ of the extended zone containing the ER difference is similar to the mean Δρ of the theoretical zone of the theoretical distribution.

For most Δρ distributions (Fig. 5), the electrical resistivity variations and single heterogeneity detection are similar for the two sequences, as is the smoothness coefficient (Table 2). However, the smoothness coefficient is higher for the GD sequence than for the DD sequence for small heterogeneity detection (Δρ distributions C1 or D3). The GD sequence appears to be less sensitive in areas distant from the electrodes than the DD sequence, which accentuates the diffusion of the information recovered by ERT inversion. It is consistent with observations in Δρ distributions E2g and E3g illustrated in Fig. 5, where the different heterogeneities are less distinguished than for the Δρ distributions obtained with the DD sequence (E2d and E3d).

3.1.2. Artifact generation

All inversion tools used for reconstructing images are known for artifact generation and information loss because the inversion may be ill-posed problem [27]. As observed in Fig. 5 and Fig. 6, negative Δρ appear next to heterogeneities. Similar heterogeneities have been observed in geophysical studies [27]. The values of negative Δρ seem related to ER differences: the higher the theoretical ER difference (with respect to the initial ER distribution) is, the higher the relative decrease in electrical resistivity next to the heterogeneity is, as observed when comparing Δρ distribution B1d with Δρ distribution B3d. However, for the experimental conditions studied, the proposed hypothesis postulates that there should not be any negative Δρ since gas injection induces an ER increase. This way, artifacts will be easily detected.

3.1.3. Conclusions of the numerical study

The potential of ERT for phase distribution analysis at large scale was numerically investigated. Heterogeneities were clearly detected for each theoretical ER distribution. For all conceptualized scenarios, the ERT is efficient to detect the evolution of electrical resistivity in terms of absolute value but also in terms of position within the studied surface. In addition, the ERT could be considered as highly sensitive to the evolution of local electrical resistivity, considering the small variations tested during the numerical study (to mimic values of local gas hold-up from 1.6 to 6.3%, consistent with previous studies in small bubbles columns or mixing vessel [40,41,20]). However, some errors mainly generated by ERT inversion for different simulated configurations are identified during this numerical study. The main ERT potential errors are summarized in Table 3.

The main identified errors are: (i) data diffusion far from electrodes, which is more pronounced for GD sequence than DD one and (ii) artifact generation close to high ER difference with initial. As expected, the numerical study allowed the evaluation and comparison of the two selected sequences of quadripole and offer information for data quality estimation for further experimental application of the ERT technique. Considering the obtained results, the DD sequence will be used for experimental ERT measurements presented in the next section.

Coupled to ERT measurement, such numerical approach is essential to optimize the experimental design in terms of electrode positions, quadripole configuration and sequences for reactor with complex internal geometries. In addition, such approach could be used in nearly future for the evaluation and application of ERT or EIT to full scale industrial reactors with complex geometries.

3.2. Experimental ERT measurements on the semi-industrial MBR

3.2.1. Activated sludge characteristics

Table 4 presents the operating conditions and the activated sludge characteristics during the ERT measurements. The shear rate in the reactor is estimated from the superficial gas and the activated sludge rheological parameters using the equation proposed by Sanchez-Perez et al. [42]. Concerning the activated sludge rheology, the obtained rheograms (not shown) confirms the non-newtonian behavior of the activated sludge for the different MLSS concentration as expected [43,25]. The activated sludge viscosity for the MLSS concentration of 3 g L^{-1} is calculated from the empirical model proposed by Duran et al. [25] for sludge from conventional activated sludge plant. In Table 4, the activated sludge viscosity was expressed at the temperature of the activated sludge measured during the experiments and for the estimated shear rate. These results illustrate the decrease in AS viscosity with an increase in the estimated mean shear rate in the reactor (associated to an increase in the air flow rate). In a same way, the AS viscosity increases with an increase in the MLSS concentration, from 3 to 10 g L^{-1}. For the different operating conditions, the apparent viscosity of the activated sludge varies from 1.3 to 4.2 mPa s^{-1}. As a complement, the activated sludge mean diameter (d_{50}) was regularly measured during the monitoring of the semi-industrial MBR. During the overall period, the measured d_{50} varies from 39 to 64 μm with a mean value of 52 μm.

3.2.2. Experimental characterization of bubble dispersion using ERT: Evaluation of the method and study of the impact of air flow rate and MLSS concentration

Fig. 7a–e presents the experimental results under the operating conditions described in Table 1 for the 1.17 m cross section. Locations of the aerated membrane modules are represented by rectangular

Table 2
Calculated smoothness coefficients (Y = yes, N = no).

Sequence	Distribution	D_{-x}	D_{+x}	D_{-y}	D_{+y}	X-centered	Y-centered
DD	B1d	1.10	1.15	1.34	1.36	Y	Y
	B2d	1.10	1.15	1.34	1.36	Y	Y
	B3d	1.10	1.15	1.34	1.35	Y	Y
GD	B1g	1.15	1.16	1.35	1.36	Y	Y
	B2g	1.15	1.16	1.35	1.36	Y	Y
	B3g	1.15	1.16	1.34	1.35	Y	Y
DD	C1d	**6.1**	**5.7**	**3.5**	**3.2**	Y	Y
	C2d	5.9	5.5	1.4	1.5	Y	Y
GD	C1g	**6.8**	**6.8**	**4.4**	**4.6**	Y	Y
	C2g	6.1	5.7	1.7	1.7	Y	Y
DD	D1d	2.7	5.0	2.8	2.7	N	Y
	D2d	2.5	4.2	1.4	1.6	N	Y
	D3d	**1.3**	**1.3**	**2.1**	**3.2**	Y	N
GD	D1g	2.9	4.9	2.7	2.8	N	Y
	D2g	2.7	4.4	1.4	1.5	N	Y
	D3g	**1.3**	**1.1**	**2.1**	**3.7**	Y	N

Table 3
Main observed ERT errors for DD and GD sequences (+ = Minor error (less than 5%)/+ + + = Major error (More than 20%).

Generated error	DD sequence	GD sequence	Associated Δρ distributions
Data diffusion close to electrodes	+	+	B1, B2, B3
Data diffusion far from electrodes	+ +	+ + +	D1, D2, D3 C1, C2
Obtained Δρ in comparison with theoretical Δρ for small (centered) heterogeneities	+ +	+ +	(C1, C2), D1, D2, D3
Obtained Δρ in comparison with theoretical Δρ for large heterogeneities	+	+	B1, B2, B3
Artifact generation for high ER difference with initial	+ +	+ +	B3, C3, D3
Artifact generation for low ER difference with initial	+	+	B1, C1, D1

Table 4
Operating conditions and activated sludge characteristics during ERT measurements.

MLSS (g L^{-1})	SAD_m ($Nm^3/h/m^2$)	T (°C)	σ ($mS.cm^{-1}$)	G (s^{-1})	μ_{app} ($mPa.s^{-1}$)
0	0.29	24	0.7	304	1.02
	0.38			349	1.02
	0.52			408	1.02
3	0.29	27	2.2	265	1.35
	0.41			320	1.31
	0.46			341	1.29
6	0.14	33	4.4	143	2.22
	0.18			167	2.10
	0.29	35	4.5	229	1.81
	0.41			283	1.67
	0.47			308	1.62
10	0.29	33	4.4	147	4.37
	0.42			194	3.64
	0.54			234	3.22

With: T = Temperature (°C), σ = conductivity ($mS.cm^{-1}$), SAD_m = specific aeration demand, the ratio between the air flow rate and membrane area in filtration ($Nm^3/h/m^2$), G the estimated shear rate using equation of Sánchez Pérez et al. [42] (s^{-1}), μ_{app} the apparent viscosity at temperature T and for the associated estimated shear rate ($mPa\ s^{-1}$).

shapes.

The results of the initial experiments (without gas injection, Column 1, Fig. 7) are presented in terms of the ratio between the electrical resistivities obtained using the ERT method and the electrical resistivity of activated sludge (or water), using a conductivity probe. Without aeration, the zone occupied by membrane modules is experimentally detected at each MLSS concentration and conductivity condition (Fig. 7, Column 1). Slight discrepancies are noted depending on the MLSS concentration and could be attributed to fiber arrangement, which is heterogeneous as mentioned in Buetehorn et *al.* [44] or possibly activated sludge properties such as floc presence, leading to slightly different configurations of fibers surrounded by sludge. Moreover, the membrane module zone seems better detected at high conductivity (low resistivity) since the results are expressed in ratio in order to facilitate the comparison of the different cases.

On Fig. 7 (Columns 2 to 4), the results are expressed in ER percentage of variation Δρ (with respect to the initial measurements without aeration). Variations in the range [−2.5%, 2.5%] are considered as the noise resulting from experimental measurement and therefore are displayed in grey.

As for numerical study results, artifacts can be observed close to zone of positive Δρ. These are more pronounced experimentally and could be related to higher Δρ values than the simulated Δρ values (45% vs 15% ER difference with initial ER, respectively). A complementary simulation was conducted by setting the electrical resistivity value of Block 2 at 6 Ω.m (results not shown here). As for experimental measurement, such artifacts (Δρ of −10%) appeared on the resulting interpreted ER model and could be attributed to inversion, which is in agreement with the previous hypothesis.

Concerning clean water Δρ distributions, a positive Δρ is observed around the zone occupied by membrane modules at high air flow rates, which is not in agreement with visual observation during experiments. A possible explanation could be a clean water conductivity decrease during the experiments (from 735 μS/cm to 694 μS/cm (6%)). For activated sludge experiments, the conductivity variation remained lower than 2%.

For all operating conditions (air flow rate and MLSS concentration), the gas is mainly localized in the membrane zone and only slight dispersion is measured around this zone. During their rising, the bubbles are confined in the membrane zone and could contribute to the fouling mitigation of the membrane by generating shear stress at the membrane surface and local movement of membrane [3]. However, the homogeneity of the local bubble dispersion mainly depends in the MLSS concentration and the injected air flow rate.

For all MLSS concentrations, an increase in the gas flow rate induces a rise in the relative increase in the Δρ within the membrane zone. This trend is similar to the gas hold-up changes observed in activated sludge in Babaei et al. [20] and is consistent with the nonconductive property of the gas phase. Maximum Δρ values are closed to 45% and higher than simulated values during the numerical study. This order of magnitude could highlight that experimental local gas hold-up is higher than maximum value considered during the numerical study (maximum value of 6.3%, corresponding to an ER variation of 10%). However, for similar gas flow rates, Δρ are higher within the membrane zone for clean water than activated sludge experiments. This second observation is in agreement with the results obtained in bubble columns filled with hardwood pulp suspension [45], xanthan gum [17] and activated sludge [20,25], where gas hold-up is lower in these fluids than in clear water. This decrease in the gas hold-up could be linked to an increase in the bubble size and in the associated bubble rise velocity, as observed by Babaei et al. [19].

For all gas flow rates, the Δρ measured for clean water and lower MLSS concentration (3 g/L) experiments highlight that bubble distribution is quite homogeneous throughout the membrane module zone (Fig. 7). For higher MLSS concentrations (6 and 10 g/L) and low/average gas flow rates, only some parts of the membrane module zone present positive Δρ, which could illustrate preferential bubble pathways. The bubble distribution over membrane modules is more homogeneous for high air flow rates. The evolving bubble pathways and distribution over the membrane module with the air flow rate could be related to the specific plastic or pseudo-plastic behavior of the activated sludge [3]. The heterogeneous distribution of the bubbles within the membrane zone is particularly pronounced for the operating conditions with the highest apparent viscosity of the liquid (from 1.7 to 4.2 $mPa\ s^{-1}$). These results confirm how the presence of the solid in sludge can participate in the production of heterogeneity; the ER distributions may help determine the extent of this phenomenon and its dependency to the sludge properties. Moreover, such observation could be useful for aeration management of MBR and the optimization of the energy consumption of MBR process at full-scale by fixing the air flow rate considering the rheological properties of the activated sludge.

For one aerated membrane module experiment (Fig. 7e), the positive Δρ values are located more around the aerated membrane module

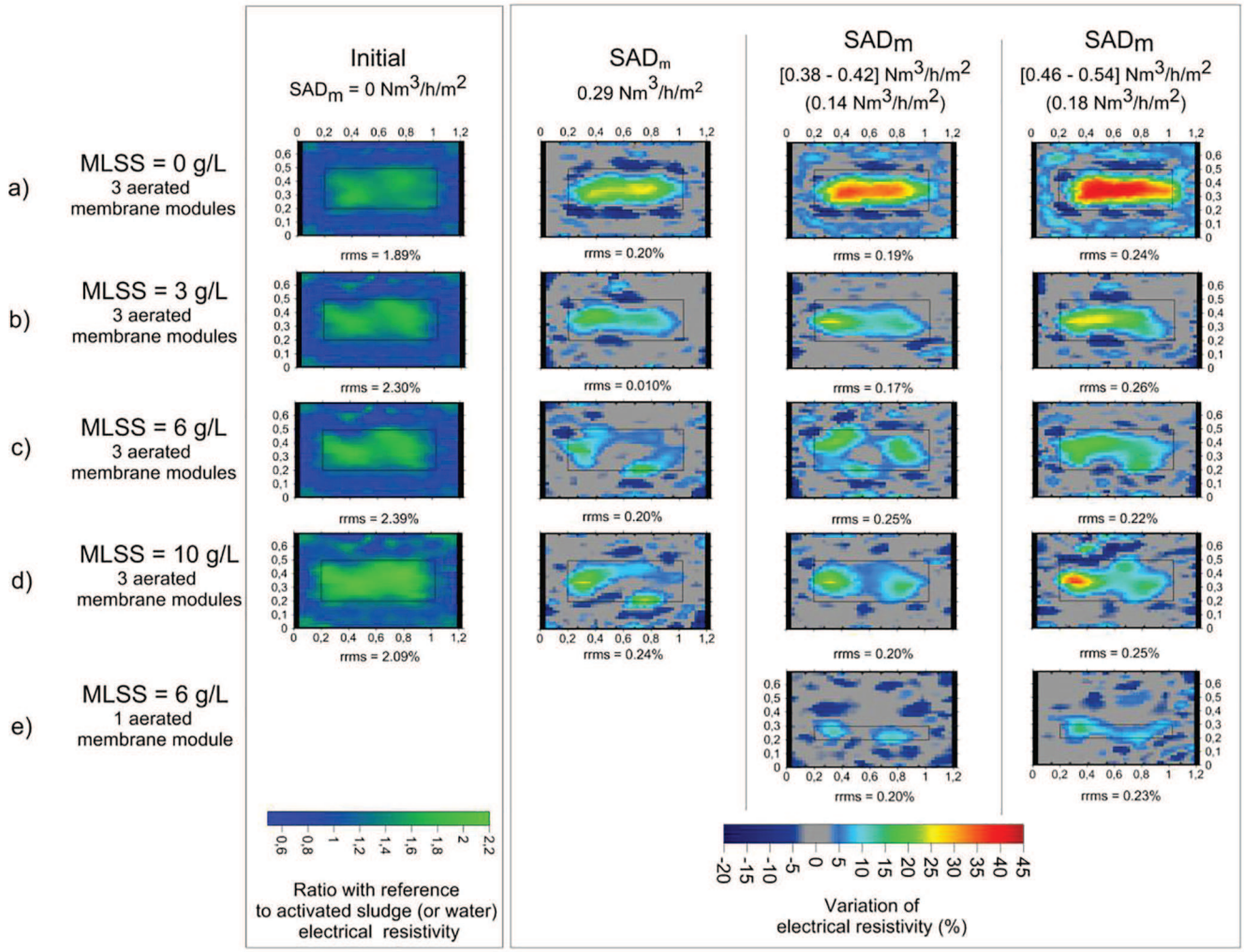

Fig. 7. Interpreted ER models (Initial – Membrane without aeration) and $\Delta\rho$ distributions for different SAD_m and MLSS concentrations: a) 3 aerated membrane modules – SAD_m = 0, 0.29, 0.38, 0.52 $Nm^3/h/m^2$ [clean water, MLSS = 0 g/L], b) 3 aerated membrane modules – SAD_m = 0, 0.29, 0.41, 0.46 $Nm^3/h/m^2$ [sludge, MLSS = 3 g/L], c) 3 aerated membrane modules – SAD_m = 0, 0.29, 0.41, 0.47 $Nm^3/h/m^2$ [sludge, MLSS = 6 g/L], d) 3 aerated membrane modules – SAD_m = 0, 0.29, 0.42, 0.54 $Nm^3/h/m^2$ [sludge, MLSS = 10 g/L], e) 1 aerated membrane module – SAD_m = 0.14, 0.18 $Nm^3/h/m^2$ [sludge, MLSS = 6 g/L] – rrms corresponds to relative root mean square error between the modeled and the experimental apparent ER distribution data sets.

than in previous experiments. These observations confirm that heterogeneities are detected by the proposed adapted ERT method in complex systems.

4. Conclusions

The objective of this work was to adapt and apply ERT to bubble dispersion characterization in a semi-industrial membrane tank filled with clear water and activated sludge.

- First, a numerical approach was proposed to define and validate the ERT methodology for the study of bubble dispersion in large-scale reactors with complex geometries. This modeling approach demonstrated the ability of the ERT method to observe gas distribution patterns for low theoretical gas hold-up in the membrane zone (from 1.6 to 6.3%). The proposed numerical study could be very useful for the development of ERT at industrial scale.
- Then, the defined ERT method was applied to the bubble dispersion characterization in a semi-industrial membrane bioreactor filled with clear water and activated sludge. The membrane module zone was well described by the measurements whatever the MLSS concentration in the case of initial experiments without aeration. Gas dispersion was more homogeneous for low MLSS concentrations (3 g/L) at low gas flow rates (SAD_m = 0.29 $Nm^3/h/m^2$). At 6 g/L and 10 g/L, a high air flow rate is required for the bubbles to be distributed on the whole membrane zone (SAD_m = 0.46 $Nm^3/h/m^2$). This result is consistent with the non-newtonian behavior of sludge.
- With current technology, the methodology presented in this paper was successfully used to adapt the ERT method and apply it to a semi-industrial MBR filled with activated sludge. The inversion parameters chosen and the sequence of quadripoles adapted presented here show promising results for observing bubble dispersion. Other inversion methods exist and could be investigated in further research. Moreover, either increasing the number of electrodes or adding electrodes at the center of the bioreactor – since in this study, the diffusive character of the distribution is the highest in this location – could improve the precision of the ERT measurement results obtained.

Acknowledgements

Authors thank the MOCOPEE program (www.mocopee.com) and Irstea for financial support. The authors wish to thank the SIAAP staff of

the Seine Aval WRRF (TDJ unit) for their availability during on-site experiments and to Irstea staff involved in the semi-industrial pilot production and on-site experiments.

References

[1] P. Krzeminski, L. Leverette, S. Malamis, E. Katsou, Membrane bioreactors – a review on recent developments in energy reduction, fouling control, novel configurations, LCA and market prospects, J. Membr. Sci. 527 (2017) 207–227.

[2] E. Akhondi, F. Zamani, K.H. Tng, G. Leslie, W.B. Krantz, A.G. Fane, J.W. Chew, The performance and fouling control of submerged hollow fiber (HF) systems: a review, Appl. Sci.-Basel 7 (8) (2017) 765.

[3] E. Braak, M. Alliet, S. Schetrite, C. Albasi, Aeration and hydrodynamics in submerged membrane bioreactors, J. Membr. Sci. 379 (1–2) (2011) 1–18.

[4] F. Wicaksana, A.G. Fane, V. Chen, Fibre movement induced by bubbling using submerged hollow fibre membranes, J. Membr. Sci. 271 (1–2) (2006) 186–195.

[5] A.P.S. Yeo, A.W.K. Law, A.G. Fane, The relationship between performance of submerged hollow fibers and bubble-induced phenomena examined by particle image velocimetry, J. Membr. Sci. 304 (1–2) (2007) 125–137.

[6] E.N.C. Duc, L. Fournier, C. Levecq, B. Lesjean, P. Grelier, A. Tazi-Pain, Local hydrodynamic investigation of the aeration in a submerged hollow fibre membranes cassette, J. Membr. Sci. 321 (2) (2008) 264–271.

[7] B.G. Fulton, J. Redwood, M. Tourais, P.R. Berube, Distribution of surface shear forces and bubble characteristics in full-scale gas sparged submerged hollow fiber membrane modules, Desalination 281 (2011) 128–141.

[8] N.Y. Liu, Q.D. Zhang, G.L. Chin, E.H. Ong, J. Lou, C.W. Kang, W.J. Liu, E. Jordan, Experimental investigation of hydrodynamic behavior in a real membrane bio-reactor unit, J. Membr. Sci. 353 (1–2) (2010) 122–134.

[9] C.C.V. Chan, P.R. Berube, E.R. Hall, Shear profiles inside gas sparged submerged hollow fiber membrane modules, J. Membr. Sci. 297 (1–2) (2007) 104–120.

[10] D. Ye, S. Saadat-Sanei, P.R. Berube, Pulse bubble sparging for the control of hydraulically reversible fouling in submerged hollow fiber membrane systems, Sep. Purif. Technol. 123 (2014) 153–163.

[11] N. Ratkovich, C.C.V. Chan, P.R. Berube, I. Nopens, Investigation of the effect of viscosity on slug flow in airlift tubular membranes in search of a sludge surrogate, Water Sci. Technol. 61 (7) (2010) 1801–1809.

[12] E. Braak, C. Albasi, D. Anne-Archard, S. Schetrite, M. Alliet, Impact of Aeration on Mixed Liquor in Submerged-Membrane Bioreactors for Wastewater Treatment, Chem. Eng. Technol. 40 (8) (2017) 1453–1465.

[13] N. Ratkovich, W. Horn, F.P. Helmus, S. Rosenberger, W. Naessens, I. Nopens, T.R. Bentzen, Activated sludge rheology: a critical review on data collection and modelling, Water Res. 47 (2) (2013) 463–482.

[14] A. Drews, Membrane fouling in membrane bioreactors-Characterisation, contradictions, cause and cures, J. Membr. Sci. 363 (1–2) (2010) 1–28.

[15] S. Buetehorn, M. Brannock, P. Le-Clech, G. Leslie, D. Volmering, K. Vossenkaul, T. Wintgens, M. Wessling, T. Melin, Limitations for transferring lab-scale microfiltration results to large-scale membrane bioreactor (MBR) processes, Sep. Purif. Technol. 95 (2012) 202–215.

[16] M. Sharifi, B. Young, Electrical resistance tomography (ERT) applications to chemical engineering, Chem. Eng. Res. Des. 91 (9) (2013) 1625–1645.

[17] E.E. Fransolet, A. Crine, P. Marchot, D. Toye, Analysis of gas holdup in bubble columns with non-Newtonian fluid using electrical resistance tomography and dynamic gas disengagement technique, Chem. Eng. Sci. 60 (22) (2005) 6118–6123.

[18] L. Pakzad, F. Ein-Mozaffari, P. Chan, Using computational fluid dynamics modeling to study the mixing of pseudoplastic fluids with a Scaba 6SRGT impeller, Chem. Eng. Process. Process Intensif. 47 (12) (2008) 2218–2227.

[19] R. Babaei, B. Bonakdarpour, F. Ein-Mozaffari, Analysis of gas phase characteristics and mixing performance in an activated sludge bioreactor using electrical resistance tomography, Chem. Eng. J. 279 (2015) 874–884.

[20] R. Babaei, B. Bonakdarpour, F. Ein-Mozaffari, The use of electrical resistance tomography for the characterization of gas holdup inside a bubble column bioreactor containing activated sludge, Chem. Eng. J. 268 (2015) 260–269.

[21] M. Audebert, R. Clement, N. Touze-Foltz, T. Gunther, S. Moreau, C. Duquennoi, Time-lapse ERT interpretation methodology for leachate injection monitoring based on multiple inversions and a clustering strategy (MICS), J. Appl. Geophys. 111 (2014) 320–333.

[22] J.E. Chambers, P.B. Wilkinson, S. Penn, P.I. Meldrum, O. Kuras, M.H. Loke, D.A. Gunn, River terrace sand and gravel deposit reserve estimation using three-dimensional electrical resistivity tomography for bedrock surface detection, J. Appl. Geophys. 93 (2013) 25–32.

[23] R. Clement, M. Descloitres, T. Gunther, O. Ribolzi, A. Legchenko, Influence of shallow infiltration on time-lapse ERT: Experience of advanced interpretation, Comp. Rend. Geosci. 341 (10–11) (2009) 886–898.

[24] M. Radulescu, C. Valerian, J.W. Yang, Time-lapse electrical resistivity anomalies due to contaminant transport around landfills, Ann. Geophys. 50 (3) (2007) 453–468.

[25] C. Durán, Y. Fayolle, Y. Pechaud, A. Cockx, S. Gillot, Impact of suspended solids on the activated sludge non-newtonian behaviour and on oxygen transfer in a bubble column, Chem. Eng. Sci. 141 (2016) 154–165.

[26] R. Clement, M. Bergeron, S. Moreau, COMSOL Multiphysics Modelling for Measurement Device of Electrical Resistivity in Laboratory Test Cell, Europeen Comsol conference, Stuttgart, 2011.

[27] R. Clement, M. Descloitres, T. Gunther, L. Oxarango, C. Morra, J.P. Laurent, J.P. Gourc, Improvement of electrical resistivity tomography for leachate injection monitoring, Waste Manage. (Oxford) 30 (3) (2010) 452–464.

[28] R. Clement, L. Oxarango, M. Descloitres, Contribution of 3-D time-lapse ERT to the study of leachate recirculation in a landfill, Waste Manage. (Oxford) 31 (3) (2011) 457–467.

[29] R. Clement, S. Moreau, How should an electrical resistivity tomography laboratory test cell be designed? Numerical investigation of error on electrical resistivity measurement, J. Appl. Geophys. 127 (2016) 45–55.

[30] M.H. Loke, Time-lapse resistivity imaging inversion, 5th meeting of the environmental and Engineering Society, European Section, Budapest, Hungary, 1999.

[31] F.D. Day-Lewis, J.W. Lane, J.M. Harris, S.M. Gorelick, Time-lapse imaging of saline-tracer transport in fractured rock using difference-attenuation radar tomography, Water Resour. Res. 39 (10) (2003).

[32] A.L. Vesnaver, F. Accaino, G. Bohm, G. Madrussani, J. Pajchel, G. Rossi, G. Dal Moro, Time-lapse tomography, Geophysics 68 (3) (2003) 815–823.

[33] T. Gunther, C. Rucker, K. Spitzer, Three-dimensional modelling and inversion of dc resistivity data incorporating topography – II. Inversion, Geophys. J. Int. 166 (2) (2006) 506–517.

[34] T. Gunther, Inversion Methods and Resolution Analysis for the 2D/3D Reconstruction of Resistivity Structures from DC Measurements (Ph.d thesis), University of Mining and Technology, Freiberg, Germany, 2004.

[35] M.H. Loke, Electrical imaging surveys for environmental and engineering studies: A Practical Guide to 2D and 3D Surveys, Unpublished Short Training Course Lecture Notes, Penang, Malaysia, 2000.

[36] E. Fransolet, M. Crine, G. L'Homme, D. Toye, P. Marchot, Analysis of electrical resistance tomography measurements obtained on a bubble column, Meas. Sci. Technol. 12 (8) (2001) 1055–1060.

[37] H.B. Jin, S.H. Yang, M. Wang, R.A. Williams, Measurement of gas holdup profiles in a gas liquid cocurrent bubble column using electrical resistance tomography, Flow Meas. Instrum. 18 (5–6) (2007) 191–196.

[38] J. Koestel, A. Kemna, M. Javaux, A. Binley, H. Vereecken, Quantitative imaging of solute transport in an unsaturated and undisturbed soil monolith with 3-D ERT and TDR, Water Resour. Res. 44 (12) (2008) 1–17.

[39] D.J. LaBrecque, M. Miletto, W. Daily, A. Ramirez, E. Owen, The effects of noise on Occam's inversion of resistivity tomography data, Geophysics 61 (2) (1996) 538–548.

[40] H. Jin, M. Wang, R.A. Williams, Analysis of bubble behaviors in bubble columns using electrical resistance tomography, Chem. Eng. J. 130 (2007) 179–185.

[41] N. Hashemi, F. Ein-Mozaffari, S.R. Upreti, D.K. Hwang, Experimental investigation of the bubble behaviour in an aerated coaxial mixing vessel through electrical resistance tomography (ERT), Chem. Eng. J. 289 (2016) 402–412.

[42] J.A. Sánchez Pérez, E.M. Rodríguez Porcel, J.L. Casas López, J.M. Fernández Sevilla, Y. Chisti, Shear rate in stirred tank and bubble column bioreactors, Chem. Eng. J. 124 (2006) 1–5.

[43] I. Seyssiecq, M. Karrabi, N. Roche, In situ rheological characterisation of wastewater sludge: Comparison of stirred bioreactor and pipe flow configurations, Chem. Eng. J. 259 (2015) 205–212.

[44] S. Buetehorn, D. Volmering, K. Vossenkaul, T. Wintgens, M. Wessling, T. Melin, CFD simulation of single- and multi-phase flows through submerged membrane units with irregular fiber arrangement, J. Membr. Sci. 384 (1–2) (2011) 184–197.

[45] L.K. Ishkintana, C.P.J. Bennington, Gas holdup in pulp fibre suspensions: Gas voidage profiles in a batch-operated sparged tower, Chem. Eng. Sci. 65 (8) (2010) 2569–2578.